Continuous wavelet analysis of coherent structures

By M. Farge[1], Y. Guezennec[2], C. M. Ho[3] AND C. Meneveau[4]

We perform an analysis of planar cuts through three-dimensional turbulent fields (planar channel flow and mixing layer) using the 2D continuous wavelet transform. We propose two new diagnostics: (a) a measure of intermittency $I(r, \vec{x})$, which is the ratio of local energy and average energy at a given scale r. (b) a local Reynolds number, defined on the local velocity contribution at a given scale, computed from the wavelet transform of the three velocity components, the scale of the transform, and molecular viscosity; this gives a representation of the local non-linearity of the flow viewed in both space *and* scale. We find, for all the analyzed flows, strong small-scale intermittency located in the ejection regions for the channel flow and in the vortex core for the mixing layer.

1. Introduction

The wavelet transform is a new technique, first introduced by Grossmann and Morlet (1984), which allows the decomposition of a signal into contributions of both space (or time) *and* scales (or frequencies). Therefore, it is particularly well suited for the study of transients or possible singular behavior of a signal. The interesting feature of the wavelet transform, as opposed to the traditional Fourier transform, is to use an analyzing function (called wavelet) which is localized in space. The scale decomposition is performed by dilating or contracting this wavelet before convolving it with the signal to be analyzed. This procedure is an optimal compromise in view of the uncertainty principle: the wavelet transform gives a very good spatial resolution for the small scales and a very good scale resolution for the large scales. As for the Fourier transform, the original signal can be reconstructed from the wavelet transform, and the energy can be computed in the wavelet space (Parseval).

Several orthonormal wavelet bases exist (Lemarie & Meyer (1986), Daubechies (1988), Mallat (1989)), which conserve information and which are, therefore, convenient from a computational point of view, especially in higher dimensions (for an application to turbulence, see Meneveau (1990)). In the present work, we explore the use of the continuous wavelet transform (which is non-orthonormal and, therefore, redundant) for the analysis of turbulent flows (Farge & Rabreau 1988). The idea is to benefit from this redundancy and observe the signal for both scale and

1 CNRS-Ecole Normale Superieure
2 The Ohio State University
3 Univ. Southern California
4 Johns Hopkins University

position in a continuous fashion; this is expected to highlight coherent structures which should display some coherence not only in physical space but also across a range of scales (for a review of the continuous wavelet transform and its applications to turbulence, see Farge (1990)). Since the continuous wavelet transform adds one more dimension to the representation, at present we will study two-dimensional cuts through three-dimensional flow fields.

The objective is to compute the wavelet transform of flow-fields resulting from direct numerical simulations of turbulent flows. First we study the velocity and temperature fields in a plane channel flow near the wall in order to measure its intermittency and to try to correlate the active regions (where energy is still high even at the small scales) with some dynamical features such as the ejections from the sublayer. We will also study the isotropy of the flow at all scales *and* locations.

Then we study the simulations of the temporal mixing layer, where the objective is to also locate the small-scale activity in the flow and to measure its intermittency. For this we study not only the wavelet transform of vorticity, velocity, and a passively convected scalar, but we also compute the local Reynolds number. This gives a good picture of the local instability of the flow, measuring the ratio of non-linearity and dissipation at every scale *and* location.

For all turbulent flows studied here, we will try, using the continuous wavelet transform, to answer the three following questions:

(1) Where are the small scales of the flow, and how intermittent are they?

(2) What is the local scaling of energy or enstrophy, and is it different from one structure to another?

(3) What is the topology of the iso-Reynolds number manifold and what is its scale extension at the dissipative level?

2. The Continuous Wavelet Transform

The discussion of the wavelet transform is done in a general setting in n dimensional space. The only constraint imposed on a function

$$\psi(\vec{x}) \in L^2(R^n),$$

(R=real numbers) to be a wavelet is the admissibility condition:

$$C_\psi = \int_{-\infty}^{\infty} \cdots \int_{-\infty}^{\infty} |\hat{\psi}(\vec{k})|^2 \frac{d^n\vec{k}}{|\vec{k}|^n} < \infty. \tag{1}$$

The function $\psi(\vec{x})$ can be either a real or complex-valued function. If $\psi(\vec{x})$ is integrable, Eq. (1) actually implies that it has zero mean:

$$\int_{-\infty}^{\infty} \cdots \int_{-\infty}^{\infty} \psi(\vec{x}) d^n\vec{x} = 0, \quad or \quad \hat{\psi}(\vec{k}=0) = 0. \tag{2}$$

From this basic wavelet, we generate the family of dilated, rotated, and translated wavelets:

$$\psi_{r,\Omega,\vec{x}'}(\vec{x}) = c(r)^{-n}\psi(\Omega^{-1}\frac{\vec{x}-\vec{x}'}{r}), \tag{3}$$

where $r \in R^+$ is a scale dilation parameter, $\Omega \in (R^n \times R^n)$ is the (unitary) rotation tensor, $\vec{x}' \in R^n$ is the translation vector, and $c(r)$ is a normalization constant. Such normalization is actually the L^2 norm if $c(r) = r^{-1/2}$, and it is the L^1 norm if $c(r) = r^{-1}$.

The analysis of the signal $f(\vec{x})$ is then given by

$$\tilde{f}(r,\Omega,\vec{x}') = \frac{1}{\sqrt{C_\psi}} \int_{-\infty}^{\infty} \cdots \int_{-\infty}^{\infty} f(\vec{x})\psi^*_{r,\Omega,\vec{x}'}(\vec{x})d^n\vec{x}. \tag{4}$$

Here ψ^* denotes the complex conjugate of ψ. In two dimensions, the rotation tensor can be characterized by a single angle θ, and there the reconstruction formula reads:

$$f(\vec{x}) = \frac{1}{\sqrt{C_\psi}} \int_{r=0^+}^{\infty} \int_{\theta=0}^{2\pi} \int_{x'=-\infty}^{\infty} \int_{y'=-\infty}^{\infty} \tilde{f}(r,\Omega(\theta),\vec{x}')\ \psi_{r,\Omega,\vec{x}'}(\vec{x})\ \frac{dr\ d\Omega(\theta)dx'dy'}{r^3}. \tag{5}$$

More of the basic properties of the wavelet transform are listed below. Here we denote the wavelet transform of a function $f(x)$ in the operator notation $W[f(x)]$ or with the tilde notation, $\tilde{f}(r,\Omega,\vec{x})$.

Linearity:

$$W[\alpha f_1(\vec{x}) + \beta f_2(\vec{x})] = \alpha\tilde{f}_1(r,\Omega,\vec{x}') + \beta\tilde{f}_2(r,\Omega,\vec{x}'). \tag{6}$$

Translation property:

$$W[f(\vec{x}-\vec{x}_0)] = \tilde{f}(r,\Omega,\vec{x}'-\vec{x}_0). \tag{7}$$

Dilation property:

$$W[f(\frac{\vec{x}}{r_0})] = \frac{1}{r_0}\tilde{f}(\frac{r}{r_0},\Omega,\frac{\vec{x}'}{r_0}). \tag{8}$$

Energy conservation:

$$\int_{-\infty}^{\infty} \cdots \int_{-\infty}^{\infty} [f(\vec{x})]^2 d^n\vec{x} =$$

$$\frac{1}{C_\psi} \int_{0^+}^{\infty} \int_{\theta_1} \cdots \int_{\theta_{n-1}} \int_{x_1'=-\infty}^{\infty} \cdots \int_{x_n'=-\infty}^{\infty} [\tilde{f}(r,\Omega,\vec{x}')]^2 \frac{dr\ d^{n-1}\Omega\ d^n\vec{x}'}{r^{n+1}}. \tag{9}$$

Characterization of the local regularity of a function:

$$|| \tilde{f}(r, \Omega, \vec{x}_0) ||_{L^1} \sim r^{\alpha}, \quad for \quad r \to 0^+, \tag{10}$$

α is the degree of differentiability of the function at $\vec{x}_0$ if $\alpha \geq 1$, or the Lipschitz exponent of the singularity present in $\vec{x}_0$ if $-1 < \alpha < 1$.

Besides the necessary admissibility condition, the choice of the analyzing wavelet is determined largely by the condition of good localization as well as smoothness in both physical and spectral space. These conditions can be expressed as

$$| \psi(\vec{x}) | < \frac{1}{1 + | \vec{x} |^n} \tag{11.a}$$

and

$$| \hat{\psi}(\vec{k}) | < \frac{1}{1 + | \vec{k} - \vec{k}_0 |^n}, \tag{11.b}$$

$\vec{k}_0$ being the dominant frequency of the wavelet, and n should be as large as possible. For instance, the Haar wavelet (similar to a French hat) is irregular in space and does not decay fast enough in spectral space; the Maar wavelet (mexican hat) is smooth in physical space, but it is not regular enough is spectral space. For the purpose of this work, we also prefer to use a complex-valued wavelet. This is because for the analysis of one-dimensional signals the phase has proven to be rich in information, e.g. to detect singularities or to compute the instantaneous frequency (Escudier & Torresani, 1988). The local energy density at every scale can then be obtained from the modulus of the complex wavelet transform.

A good compromise in terms of both space (11.a) and scale (11.b) localization is attained with the Morlet wavelet, which is a complex valued function:

$$\hat{\psi}(\vec{x}) = e^{i\vec{k}_0 \cdot \vec{x}} e^{-\frac{|\vec{x}|^2}{2}} - C_1. \tag{12}$$

Here $\vec{k}_0$ is related to the number of oscillations of the basic wavelet within the modulated region, and C_1 is a correction term that guarantees admissibility (1) by forcing the mean of ψ to be equal to zero. In our code, the wavelet is sampled in physical space, then transformed to spectral space via FFT, and the admissibility condition is satisfied by setting $\hat{\psi}(\vec{k} = 0) = 0$. The convolutions needed to evaluate the wavelet transform (Eq. (4)) are performed in Fourier space (using FFT).

Figure 1 is a plot of the 2-D Morlet wavelet for $| \vec{k}_0 | = 6$ and $\theta = 0$.

3. Intermittency function and local Reynolds Number

An unambiguous characterization of the local 'activity' of a scalar field $f(\vec{x})$ is given by the intermittency function $I(r, \vec{x})$. It is defined in terms of the wavelet transform of $f(\vec{x})$ as follows:

$$I(r, \vec{x}) = \frac{| \tilde{f}(r, \vec{x}) |^2}{< | \tilde{f}(r, \vec{x}') |^2 >_{\vec{x}'}}, \tag{13}$$

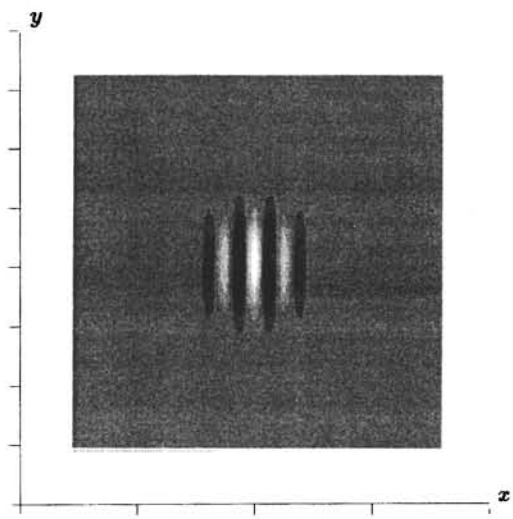

FIGURE 1. The two-dimensional Morlet wavelet, with $\theta = 0$ and $k_0 = 6$.

where the averaging extends over all points $\vec{x}'$. $I(r, \vec{x})$ then measures local deviations from the mean spectrum of a field, at every scale.

Another measure of interest is the local Reynolds number, defined in terms of the scale parameter r, the kinematic viscosity of the fluid ν, and some local root-mean-square value of the velocity field. This rms value should only correspond to contributions to the velocity field at that particular scale r. We concentrate on planar cuts through three-dimensional fields, but still consider all three velocity components on that cut. Let $\tilde{u}_i(r, x, y, \theta)$ be the continuous (2D) wavelet transform of the ith component of the fluctuating part of the velocity field in the plane of the cut, defined as follows:

$$\tilde{u}_i(r, x, y, \theta) = \frac{1}{\sqrt{C_\psi}} \int_{-\infty}^{\infty} \int_{-\infty}^{\infty} u_i(x', y')\, \psi^*_{r,\theta,x,y}(x', y')\, dx'\, dy'. \tag{14}$$

From here on we concentrate on a single angle, say $\theta = 0$, $\theta = \pi/2$, or the value of the wavelet coefficients averaged over 16 different angles equally sampled in $[0, 2\pi]$. The total kinetic energy can be obtained from

$$\frac{q^2}{2} = \frac{1}{2} \int_{r=0+}^{\infty} \int_{x=-\infty}^{\infty} \int_{y=-\infty}^{\infty} \tilde{u}'(r, x, y)^2\, \frac{dx dy dr}{r^3}, \tag{15}$$

where

$$\tilde{u}'(r, x, y) = \sqrt{\frac{1}{3C_\psi}[\tilde{u}_1(r, x, y)^2 + \tilde{u}_2(r, x, y)^2 + \tilde{u}_3(r, x, y)^2]}. \tag{16}$$

Here $\tilde{u}'(r,x,y)$ is the characteristic rms velocity at scale r and at location (x,y) in the plane being analyzed. Now we can define the local Reynolds number at every scale, according to

$$Re(r,x,y) = \frac{\tilde{u}'(r,x,y)\, r}{\nu}. \tag{17}$$

The expectation is that at large scales $r \sim L$, the Reynolds number should roughly coincide with the usual large-scale Reynolds number $Re = u'L/\nu$, where u' is the rms turbulent velocity and L is some integral scale of the flow. At the smallest scales (say $r \sim \eta$, where η is the Kolmogorov scale of the flow), one would expect this Reynolds number to be close to unity. The question we want to address here is about the variability of such a Reynolds number defined locally in space *and* scale. That is, are there locations where such a Reynolds number at some small scale is much larger than in others, and how such regions correlate with regions of small-scale activity in the flow? If so, then this could be a measure of the non-linearity at small scales (or at any desired scale); it is unambiguous because it is based on energy considerations. Such regions of high local Reynolds number could then also be interpreted as regions of strong non-linearity within the flow.

As mentioned in section 2, we utilize the Morlet wavelet to perform the analysis. In addition to location *and* scale, the angle of the wavelet can also be prescribed. For notational convenience we omit explicit reference to this angle when using $\theta = 0$ (with respect to the x-axis). When using another angle, we indicate this by adding another variable, e.g. $Re(r,x,y,\theta)$. Another issue of importance when computing the local Reynolds number is the precise value of the constant C_ψ. In the continuous case it is given by Eq.(1). However, in practice the convolutions needed to obtain the wavelet transform will be done discretely, which means that some discretization error is unavoidable. To obtain an effective constant C_ψ such that energy is the same in the physical and wavelet spaces, we compute C_ψ from

$$C_\psi = \frac{\int_{0+}^{\infty}\int_{-\infty}^{\infty}\int_{-\infty}^{\infty} [\tilde{u}_1(r,x,y)^2 + \tilde{u}_2(r,x,y)^2 + \tilde{u}_3(r,x,y)^2]\, \frac{dxdydr}{r^3}}{\int_{-\infty}^{\infty}\int_{-\infty}^{\infty} [u_1(x,y)^2 + u_2(x,y)^2 + u_3(x,y)^2]\, dxdy}. \tag{18}$$

This is then used to obtain $\tilde{u}'(r,x,y)$ (16) and $Re(r,x,y)$ (17).

4. Analysis of near-wall dynamics in turbulent channel flow

In this section, we analyze a turbulent channel flow at a Reynolds number $Re_\tau = 180$. In addition to the velocity field, three passive scalars (heat for $Pr = 0.1$, 0.7, 2.0) are also computed for the case where one wall is uniformly hot and the other is uniformly cold. Both the hydrodynamics and the scalar fields are fully developed. For more details about the flow characteristics and the computation, see Kim and Moin, 1989. In this report, we will concentrate solely on the analysis of the velocity component normal to the wall, the temperature for $Pr = 0.7$ and the pressure.

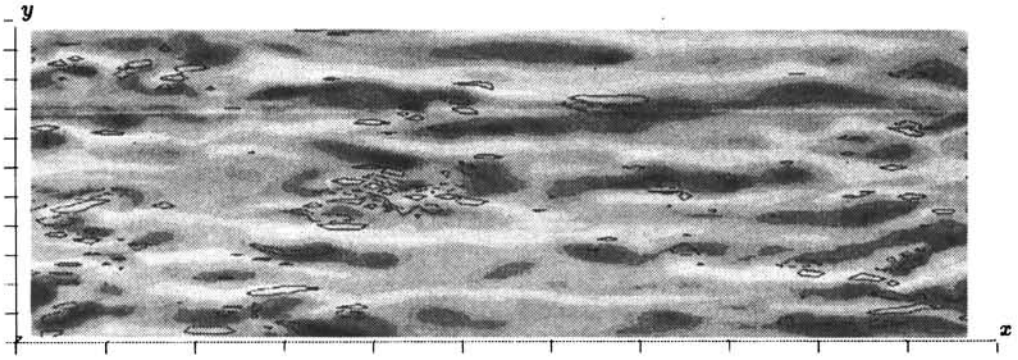

FIGURE 2. Iso-temperature lines in a horizontal x-z plane at $y^+ = 10$, in the plane channel flow simulation. Black spots indicate regions of high values of the normal velocity.

Since the wall region is the most active dynamically, the analysis is focused on one single plane, parallel to the wall at $y^+ = 10$. Figure 2 shows iso-lines of temperature in that plane. Black regions indicate the maxima of the normal velocity field. While the normal velocity is the one responsible for the advection of heat from the wall, the two fields exhibits a very different character. The temperature field is very streaky, while the regions of active transfer from or to the wall are very localized.

Next we compute the continuous wavelet transform of the temperature field for $\theta = 0$ and for scales ranging from $r = 64$ to $r = 4$ (in units of the elementary computational grid). In all subsequent figures, the r-axis is logarithmic (the small scale r=4 on the top and the large scales r=64 on the bottom). We consider 40 steps for the discretization of r, which means a base of 1.074 for the logarithmic increments. In Fig. 3, we show the intermittency factor $I(r, x, z)$, defined as the energy (modulus squared) of the wavelet coefficients normalized at every scale on the average energy at that scale (13). We observe the following features:

(a) In the large scales, the energy is evenly distributed in space.

(b) On the contrary, the temperature field at the small scales is highly intermittent; in four locations at the smallest scale, the local energy is about 15-20 times the average energy at that scale.

(c) The flow remains anisotropic, with similar elongation factor at all scales.

Let us then compare the wavelet transform of the temperature field with the one of normal velocity. Figures 4 and 5 show the wavelet transforms in the x-z plane, where the r-dependence has been compressed; this representation is analogous to viewing the wavelet coefficients as in Fig. 3 from 'above', parallel to the r-axis. In Fig. 4, we use the transform with $\theta = 0$, which selects the streamwise contributions, while in Fig. 5, we use $\theta = \pi/2$, which selects the spanwise contributions to the fields. In both figures, we plot the transform of the temperature (4(a) and 5(a)) and the transform of the normal velocity (4(b) and 5(b)).

We observe that regions of activity in the temperature field are correlated with

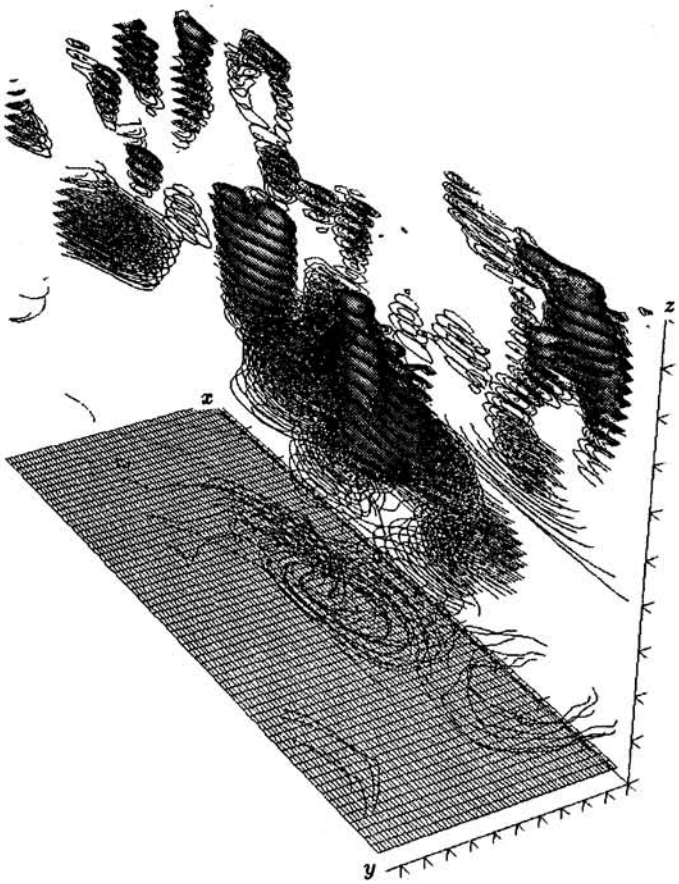

FIGURE 3. Wavelet transform of temperature field for $\theta = 0$ in plane channel flow at $y^+ = 10$.

the spots where vertical velocity is high. These regions correspond to ejections from the viscous sublayer. In the case $\theta = 0$, it is interesting to notice that even though the streaks are elongated in the streamwise direction, the wavelet transform shows some very localized active regions. This, therefore, indicates strong local changes in the x-direction inside or at the end of the streaks. These events are also correlated with the peaks of vertical velocity (Fig. 2). This is probably due to the fact that the temperature, as the streamwise velocity streaks, are very passive almost everywhere, except in very localized regions associated to the ejection mechanism. In other words, this intermittency function allows to locate very precisely the regions characterized by strong dynamics.

In the spanwise direction (considering $\theta = \pi/2$) we observe similar correlation between temperature and normal velocity; however, the activity is less intermittent. The maximum value of $I(r, x, z)$ for this case is 13 for the temperature, and 18 for

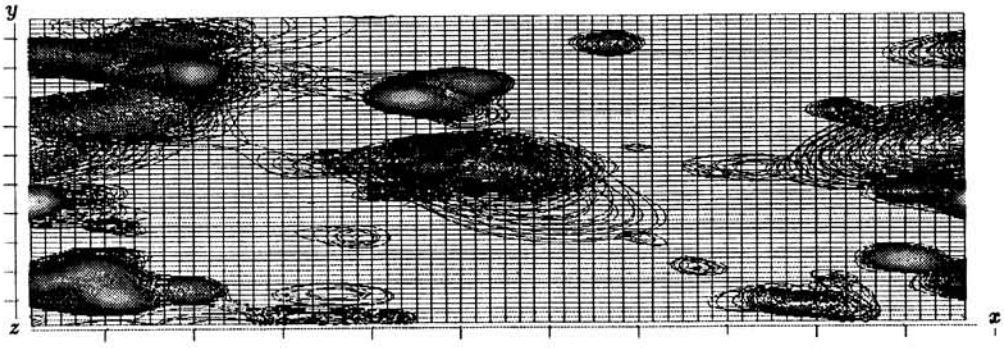

FIGURE 4(A). Intermittency function $I(r, x, z)$ of temperature field in plane channel flow at $y^+ = 10$, in the direction $\theta = 0$. Shown are iso-lines of $I(r, x, z)$ ranging from $I = 2$ to $I = 20$.

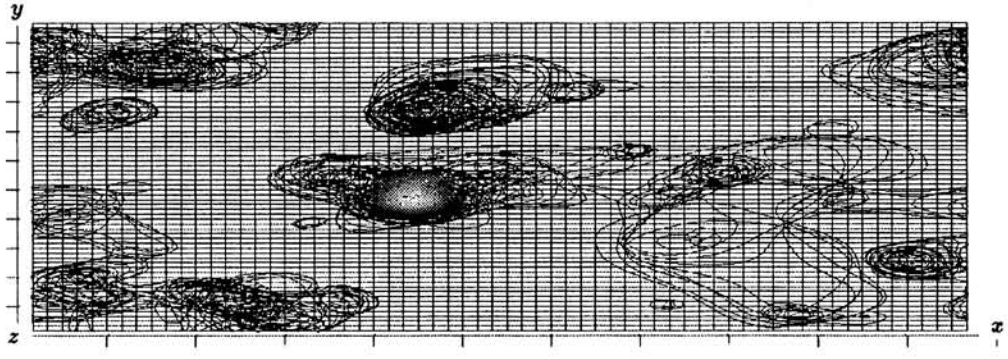

FIGURE 4(B). Intermittency function $I(r, x, z)$ of normal velocity field in plane channel flow at $y^+ = 10$, in the direction $\theta = 0$. Shown are iso-lines of $I(r, x, z)$ ranging from $I = 2$ to $I = 46$.

the vertical velocity, while for the streamwise direction it is respectively 20 and 46.

We now turn our attention to the pressure field in the same plane. Fig. 6 depicts the pressure fluctuations at $y^+ = 10$, highlighted with the regions of strong normal velocity. Despite the integral character of the pressure, the pressure fluctuations tend to be very spotty and concentrated primarily in the regions with strong normal velocity perturbations.

The transform of the pressure field is shown in Figure 7a and 7b for the streamwise ($\theta = 0$) and spanwise ($\theta = \pi/2$) directions, respectively.

The intermittency values in the spanwise and streamwise directions are similar in distribution and magnitude. As noted before, the pressure fluctuations are relatively homogeneous at the large scales and highly intermittent at the small scales.

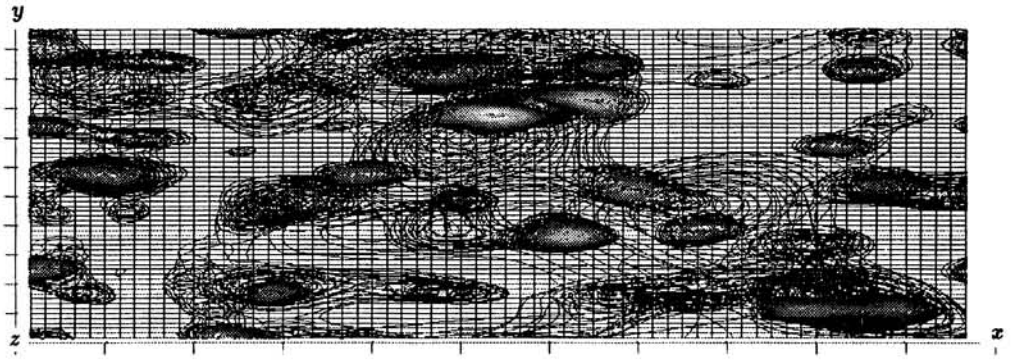

FIGURE 5(A). Intermittency function $I(r,x,z)$ of temperature field in plane channel flow at $y^+ = 10$, in the direction $\theta = \pi/2$. Shown are iso-lines of $I(r,x,z)$ ranging from $I = 1$ to $I = 13$.

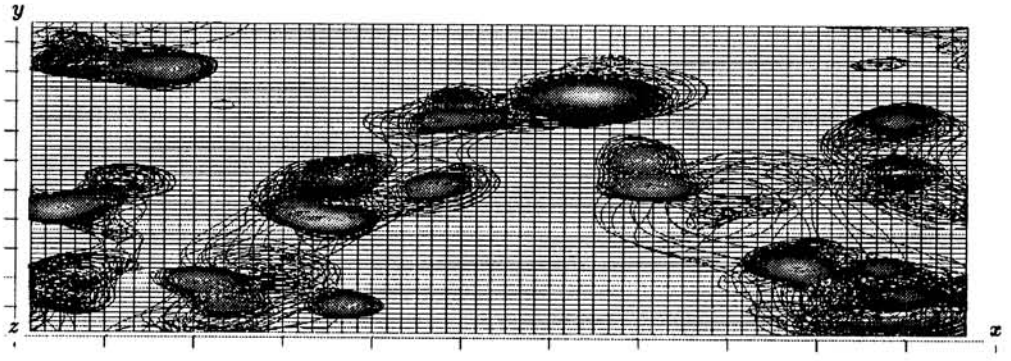

FIGURE 5(B). Intermittency function $I(r,x,z)$ of normal velocity field in plane channel flow at $y^+ = 10$, in the direction $\theta = \pi/2$. Shown are iso-lines of $I(r,x,z)$ ranging from $I = 2$ to $I = 18$.

Furthermore, the anisotropy of the small scales observed for the temperature and normal velocity is also present for the pressure fluctuations, and it appears that the elongation in the streamwise direction remains similar over a significant range of scales. Again, regions of high intermittency for the pressure can be correlated with regions of strong ejections (normal velocity away from the wall) which set up strong streamwise and spanwise local pressure gradients. This confirms the importance of these localized pressure gradients for "momentum mixing" as discussed by Guezennec *et al.* (1990). As pointed out earlier, this intermittency is very useful in pinpointing the regions dominated by strong dynamics.

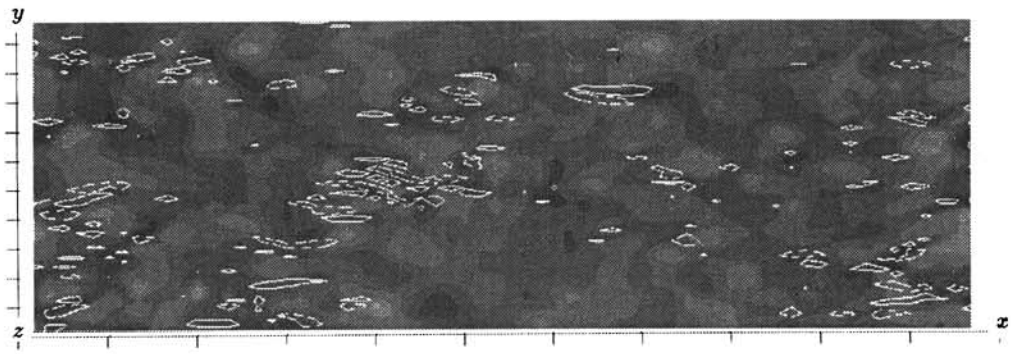

FIGURE 6. Iso-lines of pressure in the x-z plane at $y^+ = 10$ in the plane channel simulation. Black spots indicate regions of high values of the normal velocity.

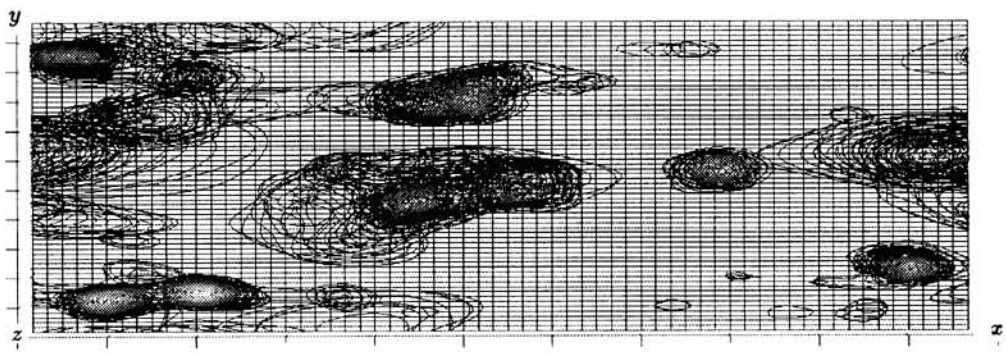

FIGURE 7(A). Intermittency function $I(r, x, z)$ of pressure field in plane channel flow, in the direction $\theta = 0$. Shown are iso-lines of $I(r, x, z)$ ranging from $I = 2$ to $I = 22$.

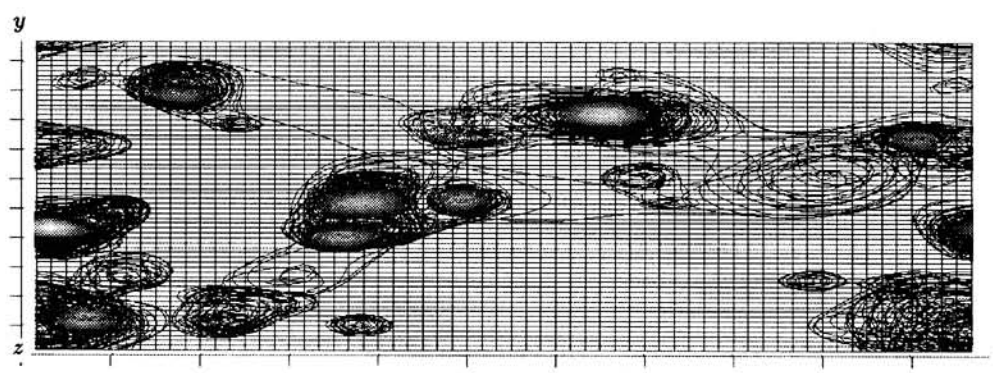

FIGURE 7(B). Intermittency function $I(r, x, z)$ of pressure field in plane channel flow, in the direction $\theta = \pi/2$. Shown are iso-lines of $I(r, x, z)$ ranging from $I = 2$ to $I = 26$.

5. Analysis of mixing layer

In this section, we perform the continuous wavelet analysis of numerical simulations of the temporally evolving mixing layer by Rogers & Moser (1990). The fields analyzed correspond to the vortex produced after the first merging (namely after the mixing transition). We consider a cut in the horizontal direction going through the center of the core region. Iso-lines of vertical (w_y) vorticity are shown in Fig. 8. The center of the plot corresponds to the spanwise vortex core. The alternating sign vortical structures seen on either side of the plot represent cuts through the "ribs" (the streamwise vortices formed between the vortex cores).

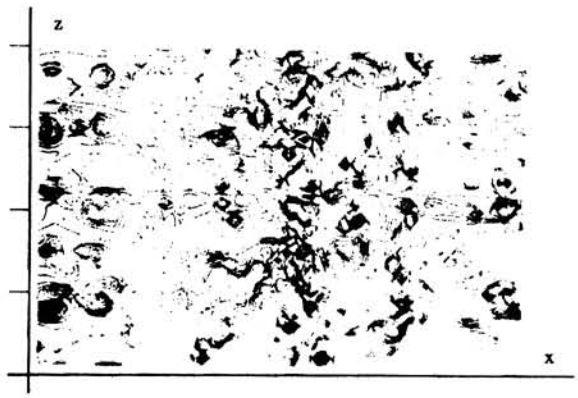

FIGURE 8. Vorticity contours in a x-z plane in the mixing layer (Rogers & Moser, 1990).

We compute $\tilde{u}_1(r,x,z)$, $\tilde{u}_2(r,x,z)$ and $\tilde{u}_3(r,x,z)$, the two-dimensional wavelet transform of this field for each velocity component u_1 (streamwise), u_2 (vertical) and u_3 (spanwise).

We also compute the wavelet transform of the vertical vorticity component, for which we plot the intermittency function $I(r,x,y)$ defined in section 2 (13) giving for each scale the local deviations of the modulus around the spectral mean value. Such representations of the transform are shown in Fig. 9.

The following conclusions regarding vorticity can be reached:

(a) The large-scales are evenly distributed in space.

(b) There is a very strong intermittency (reaching a factor $I = 120$) of the small scales and these are localized in the vortex core.

(c) We observe return to isotropy at the small scales (such a conclusion is drawn from combining both figures 9(a) and 9(b))

We now analyze the velocity fields. Figures 10(a), (b) and (c) show $I(r,x,z)$ for each velocity component, again viewed by 'collapsing' the r-axis. It is clear that the active zones of the streamwise velocity (Fig. 10(a)) are localized in a narrow region along the centerline of the vortex core and they are highly intermittent (the maximum value of $I(r,x,z)$ reaches 145). The spanwise component (Fig. 10(b)) has

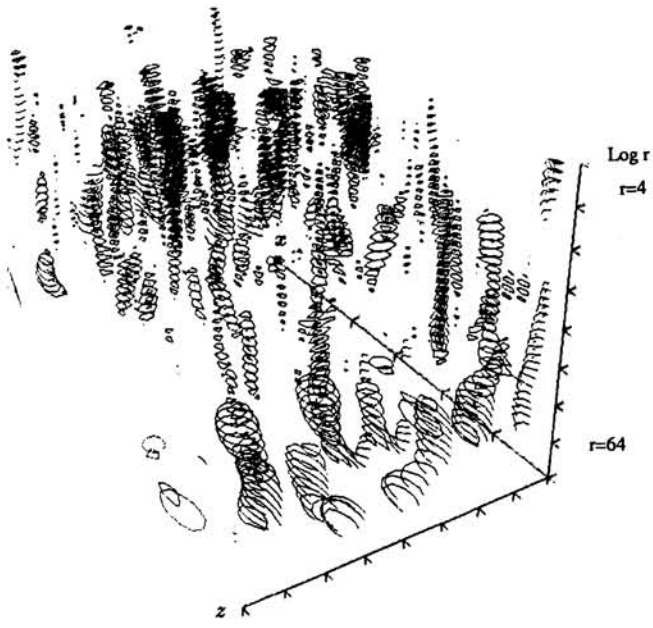

FIGURE 9(A). Intermittency function $I(r, x, z)$ of the vertical vorticity component in the mixing layer.

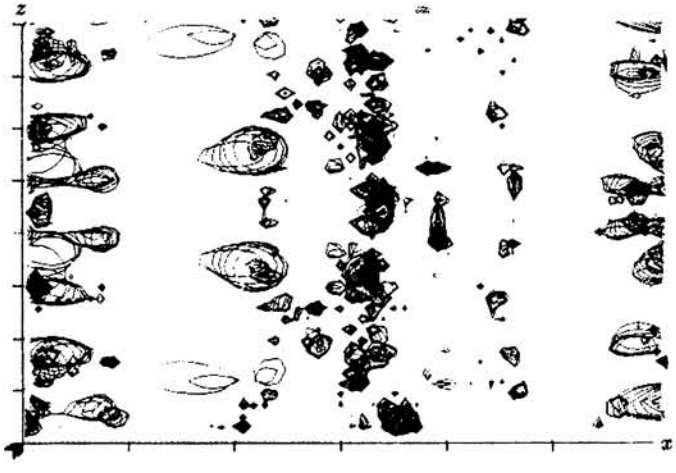

FIGURE 9(B). Intermittency function $I(r, x, z)$ of the vertical vorticity component in the mixing layer, viewed from 'above'. Shown are iso-lines of $I(r, x, z)$ ranging from $I = 0$ to $I = 125$.

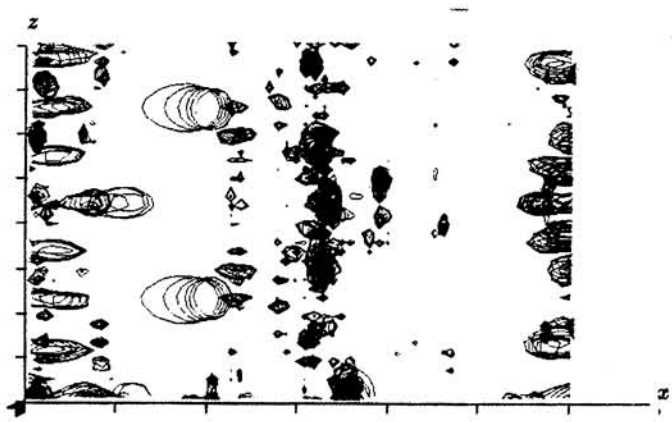

FIGURE 10(A). Intermittency function for the streamwise (u_1) velocity component in the mixing layer (top view, parallel to r-axis). Shown are iso-lines of $I(r, x, z)$ ranging from $I = 0$ to $I = 145$.

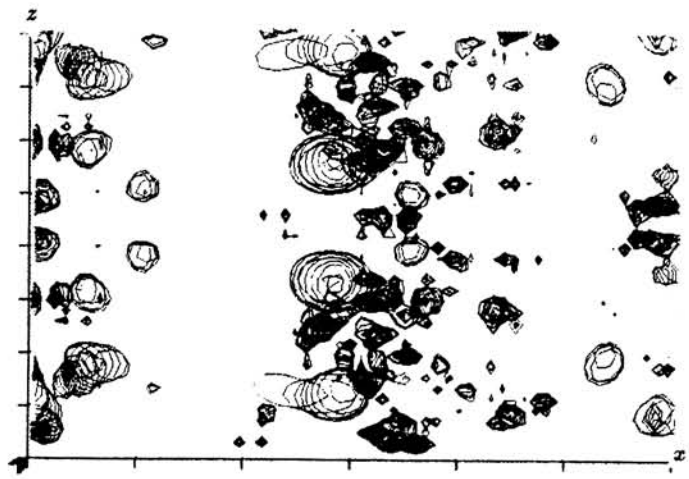

FIGURE 10(B). Intermittency function for the spanwise (u_2) velocity component in the mixing layer (top view, parallel to r-axis). Shown are iso-lines of $I(r, x, z)$ ranging from $I = 0$ to $I = 90$.

activity also localized in the vortex core, but in a wider zone, and it is less intermittent ($I(r, x, z)$ reaches at most 90). On the contrary, the vertical velocity component (Fig. 10 (c)) is much more space-filling and considerably less intermittent ($I(r, x, z)$ maximum is 40).

Now we consider two spanwise cuts (constant x) of the intermittency function. The first cut is located in the braid region, while the second corresponds to the vortex core. These cuts (not shown here) were obtained for each velocity component.

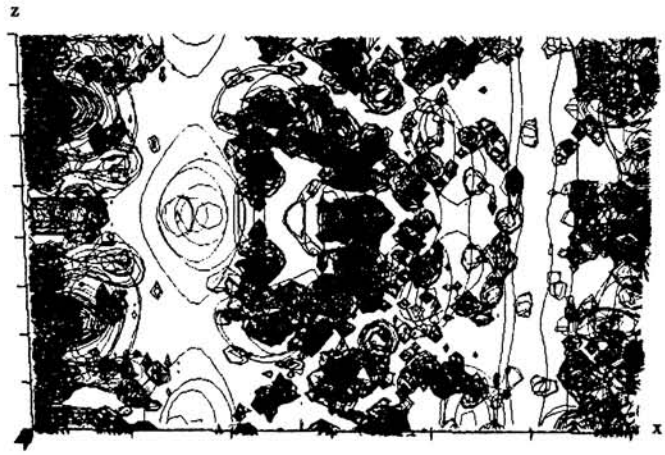

FIGURE 10(c). Intermittency function for the vertical (u_3) velocity component in the mixing layer (top view, parallel to r-axis). Shown are iso-lines of $I(r, x, z)$ ranging from $I = 0$ to $I = 40$.

As a first conclusion, we state that the intermittency in the braid regions is very low (between 0 and 5), this at every scale. Second, in the vortex core we observe different features comparing the three velocity components:

(a) For the streamwise component, only one relevant small-scale structure is visible, for which $I(r, x, z) = 85$. Its fluctuations exist on a band of scales corresponding to $r \sim 16$ to the smallest resolved scales ($r = 4$).

(b) For the spanwise component, the small-scale activity is more distributed, occurring only at the smallest scales (around $r \sim 4$. The maximum intermittency there is 40, and is encountered at three different locations, possibly corresponding to some ribs (Moser & Rogers 1990) engulfed into the vortex core.

(c) For the vertical velocity component, we observe a very different behavior: The intermittency is weak (maximum value of I is 9), and is encountered in two distinct bands of scales (around $r \sim 16$ and $r \sim 4$), separated by a clear gap with no activity there. Within the active bands, we can distinguish several features which we interpret tentatively as the cups region (Moser & Rogers 1990), or again ribs engulfed into the vortex core.

Similar conclusions concerning the small scale activity concentrated in the core region and the difference between different velocity components were reached with a technique called 'peak-valley counting' utilized by Zohar *et al.* (1990). This technique provides information about the geometry of scales but not about their energy content.

From the computation of the wavelet coefficients, we can also plot local spectra, defined as $\mid \tilde{f}(r, x_0, z_0) \mid^2$ the energy or enstrophy at some location (x_0, z_0) as a function of scale, plotted in terms of inverse scale r^{-1}. As an example, we study the local spectra of the vertical vorticity at three different points: The two points where vorticity is largest (these are actually located in the vortex core), and a point

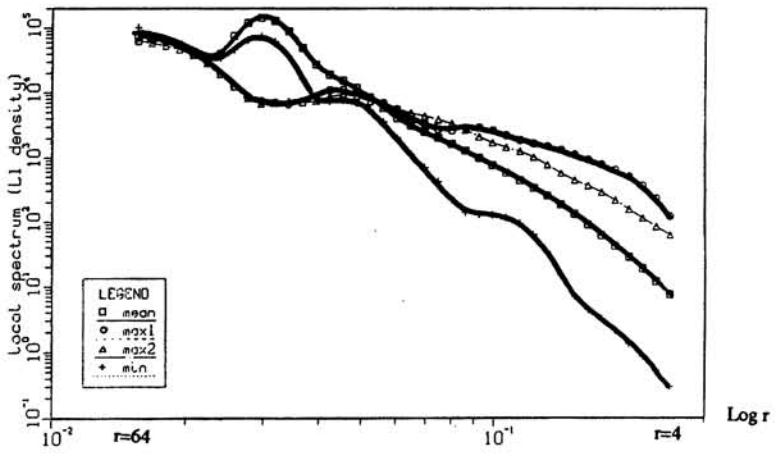

FIGURE 11. Comparison of global and local spectra of vertical vorticity in the mixing layer. The squares correspond to the spectral mean over all locations. The crosses correspond to the local spectrum at the location of very small vorticity in the braid region. The circles correspond to the local spectrum at the location of maximum vorticity (in the core region), and the triangles correspond to the second maximum of vorticity, also located in the core region.

(located in the braid region) where vorticity is very low. We also compute the average enstrophy (average over all points (x, z) for each scale). The results are plotted in Fig. 11.

For scales smaller than r=20, we observe a rapid departure from average, a sign of the strong intermittency. At the scale $r = 4$, the difference is 1.4 decades in enstrophy. Extrapolating the spectra using the observed slopes, we conjecture that the larger the Reynolds number, the larger the degree of intermittency.

As a next step, we analyze the distribution of local Reynolds number, which is defined combining all three velocity components. In Fig. 12 we show a iso-Reynolds number surface corresponding to $Re = 25$. This can be interpreted as a surface of iso-level of nonlinearity in the flow. It is not flat and it presents a scale extension over 4 octaves ($r = 64$ to 4). Its peaks, corresponding to the most unstable regions, are located in the vortex core, clearly confirming our previous conclusions concerning the small-scale activity there.

In the vortex core, relatively high local Reynolds numbers are attained at much smaller scales in the braid region (we notice that $Re = 25$ even reaches the smallest computed scale $r = 4$). Due to the limited resolution of the data, we have not obtained the manifolds for Reynolds numbers smaller than 5. Therefore, we have not attained the dissipative manifold $Re = 1$, but it is safe to argue that the dissipative manifold would also fluctuate, meaning that the Kolmogorov scale varies with location, being much smaller in the vortex core than in the braid regions.

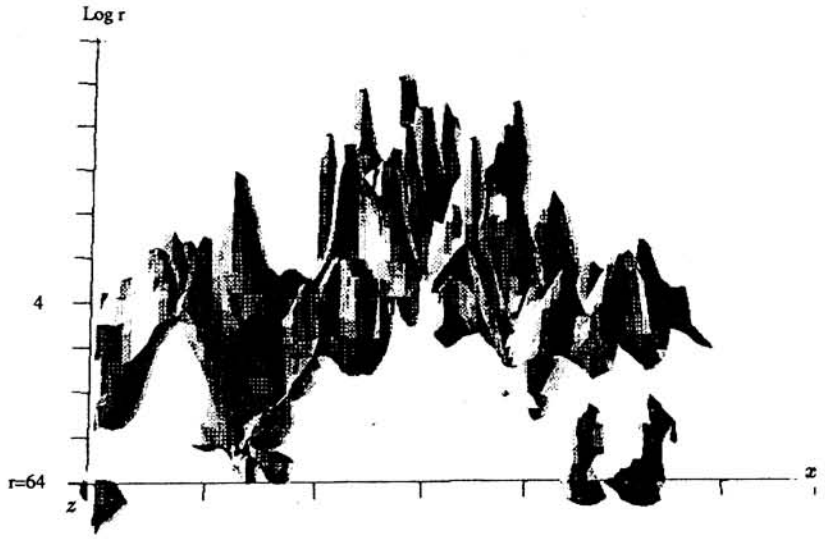

FIGURE 12. Local Reynolds number behavior in the mixing layer. Shown is a surface corresponding to $Re(r, x, z) = 25$. The peaks are located in the vortex core.

6. Conclusions

In conclusion, the wavelet transform allows us to:

(1) Localize the dynamically active regions of a turbulent flow.

(2) In varying the wavelet angle θ, we are able to separate the streamwise contributions (for $\theta = 0$) from the spanwise contributions (for $\theta = \pi/2$) of the flow field we analyze.

(3) In comparing the isotropy of the flow at different scales, we can test the return to isotropy in the small scales.

In order to answer the three questions we have asked in the introduction, we have defined three new diagnostic tools:

(1) A measure of intermittency, defined as the ratio of local energy to average energy at a given scale,

(2) A local spectrum giving the energy or enstrophy distribution versus scale in the vicinity of a given point, which can then be compared to the total spectrum,

(3) A local Reynolds number, defined in terms of the local velocity contribution, the scale of the transform, and molecular viscosity. This gives a representation of the local non-linearity of the flow viewed in both space *and* scale. The surface $Re = 1$ corresponds to the 'dissipative manifold' and its topology (flat or not) indicates how much the Kolmogorov scale varies in space.

For all flows considered we have found that:

(1) In the large scales, the energy density is homogeneous,

(2) In the small scales, the energy density is very inhomogeneous, and there is a strong intermittency associated to some coherent structures, namely the "bursts"

for the channel flow and the vortex core for the mixing layer,

(3) The topology of iso-Reynolds number surfaces is not flat and their peaks, corresponding to the most unstable regions, are encountered in the vortex core of the mixing layer, where the Kolmogorov scale is, therefore, much smaller than in the rest of the flow.

Finally, as future development, the continuous wavelet transform in two dimensions (as opposed to the one-dimensional case which has received much attention) needs to be tested more in detail in some simple test cases. One needs to better understand the information given by the phase, define better techniques to average over angles, and compare results using different wavelets (orthogonal or not).

Acknowledgements

The authors wish to thank: M. Holschneider, from the Center for Theoretical Physics, CNRS-Luminy, who has contributed to the writing of the two-dimensional wavelet code; R. Moser and M. Rogers, NASA Ames, for making their mixing-layer database available for analysis, and J. Kim and P. Moin for sharing the channel-flow data.

REFERENCES

DAUBECHIES, I. 1988 *Comm.Pure Appl. Math.* **XLI**, 909

FARGE, M. 1990 in Annual Conference of the Societe de Mathematiques de France

FARGE, M. AND RABREAU, G. 1988 *C. R. Acad. Sci. Paris* **II 307**, 1479

GROSSMANN, A. AND MORLET, J. 1984 *SIAM J. Math. Anal.* **15**, 723

GUEZENNEC, Y., STRETCH, D. AND KIM, J. 1990 This Volume (see also APS Abstracts)

MALLAT, S. J. 1989 *IEEE Patt. Anal. and Mach. Int.* **11**, 674

KIM, J. AND MOIN, P. 1989 Turbulent Shear Flow **6**, 85

LEMARIE, P. G. & MEYER, Y. 1986 *Rev. Mat. Ibero-americana* **2**, 1

MENEVEAU, C. 1990 *CTR Manuscript 120,* Center for Turbulence Research NASA Ames/Stanford

MOSER, R. D.& ROGERS, M. M. 1990 IUTAM Symp. on Stirring and Mixing

ZOHAR, Y., BUELL, J. C., MOSER, R. D., & HO, C. M. 1990 This Volume (see also APS Abstracts)